ASCAT Soil Moisture Report Series No. 11

WARP5.0
Error Analysis 1

VIENNA
UNIVERSITY OF
TECHNOLOGY

INSTITUTE OF
PHOTOGRAMMETRY
AND REMOTE SENSING

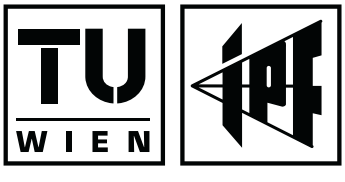

September 2006

How to reference this report:

Naeimi V. (2006), *WARP5.0 Error Analysis 1.* ASCAT Soil Moisture Report Series, No. 11, Institute of Photogrammetry and Remote Sensing, Vienna University of Technology, Austria.

Contact Information:

Institute of Photogrammetry and Remote Sensing (I.P.F.)
Remote Sensing Group
Vienna University of Technology
Gusshausstrasse 27-29/E122
1040 Vienna, Austria

microwave@ipf.tuwien.ac.at
www.ipf.tuwien.ac.at/radar

Status:	Issue 1.0
Author:	IPF TU Wien (VN)
Circulation:	IPF, EUMETSAT
Amendments:	

Issue	***Date***	***Details***	***Editor***
Issue 1.0	2006 Sep. 10	Initial Document.	VN

If further corrections are required please contact Vahid Naeimi. (vn@ipf.tuwien.ac.at).

List of Symbols and Acronyms

σ^0	Backscattering coefficient (dB)
σ^0_{noise}	Backscattering coefficient of noise signal (dB)
σ'	First derivative of σ^0 (slope) (dB/degree)
δ	Difference of σ^0 measured by the fore and aft beam antennas (dB)
δ_H	Weighted value of δ using Hamming function (dB)
γ	Normalized backscattering coefficient (dB)
Kp	Radiometric resolution (dB)
covar	Covariance
H	Hamming function
$StDev$	Standard Deviation
var	Variance
ASCAT	Advanced Scatterometer
DGG	Discrete Global Grid
ERS	European Remote Sensing Satellite
ESCAT	ERS Scatterometer
ESD	Estimated Standard Deviation
METOP	Meteorological Operational satellite
RF	Radio Frequency
TU Wien	Vienna University of Technology
WARP	WAter Retrieval Package

Contents

List of Symbols and Acronyms ii
Contents iii
1 Introduction 1
2 Scatterometer Noise Measurement 3
2.1 Radiometric Resolution 3
2.2 Noise Model 4
2.2.1 Azimuthal Anisotropy 5
2.2.2 Estimated Standard Deviation of σ^0 5
2.2.3 Spatial Correlation of Measurements 7
2.2.4 Using Hamming Window in ESD Calculations 11
2.2.5 Noise of Azimuthally Corrected Measurements 12
3 Error Sources Definition 14
3.1 Instrument Noise 14
3.2 Geophysical Error Sources 15
3.2.1 Mountains 15
3.2.2 Water 16
3.2.3 Desert Dunes 18
Bibliography 20

1 Introduction

Scatterometers onboard ERS and METOP satellites are radars operating at C-Band. They have a set of 3 antennas with look angles of 45° forward (*fore*), backward (*aft*) and to the side (*mid*) with respect to the satellite's track (METOP scatterometer has 2 sets of 3 antennas on each side). The scatterometers illuminate the Earth's surface with a group of radio frequency (RF) pulses and measure the total energy of the backscattered signal. The backscattering coefficient σ^0 measured by scatterometers depends on roughness and dielectric properties of the surface as well as the look direction of the sensor. The received scatterometer signals composed of backscattered radiation, and instrument noise in addition to the geophysical noise which is not related to the transmitted pulse. The primary application of scatterometers is to measure wind speed and direction over the ocean. But in recent years scatterometer data was also found practical in land and ice surface studies. An attractive land application of scatterometers is their ability to detect soil moisture variations. A soil moisture retrieval model using a change detection method based on the long-term scatterometer data was presented by (Wagner 1998). On the basis of this model a processing software package called WARP (soil WAter Retrieval Package) is developed at the Institute of Photogrammetry and remote Sensing (IPF) at Vienna University of Technology (TU Wien).

The degree of accuracy and reliability of the soil moisture product calculated in WARP depends on the retrieval algorithm functionality and the noise of the scatterometer measurements. Knowledge of the noise level of each measurement gives us a better understanding of the final soil moisture product.

This study consists of two parts. In the first part an analytical discussion about noise of measurement is presented introducing a quantitative noise model. A chapter in this part of report is also dedicated to the definition of error sources. By means of the noise model, which is based on azimuthal anisotropy, the most probable errors are detectable in scatterometer measurements. However, some non-systematic error sources resulting from snow cover and frozen surfaces remain unpredictable, which cause uncertainties in soil moisture estimation. These errors are not detectable with this model and should be masked externally. The estimated azimuthal noise of measurements, which is obtained from about 10 years ERS-scatterometer data, builds a basis in noise model for the error propagation through TU Wien algorithm to

obtain the noise of soil moisture measurements, which is the subject of the second part (Naeimi 2007) of the report.

2 Scatterometer Noise Measurement

2.1 Radiometric Resolution

Backscattering signals measured by scatterometers are affected by instrument noise as well as noise resulting from geophysical phenomena. To improve the instrument accuracy, the receiver noise power is measured separately and then subtracted from the backscattered signal. The noise measurements and system calibration are obtained within a dwell period between the transmission of each pulse and the arrival of the first radar echo signal (Attema 1991). A commonly used parameter for evaluation of the backscattering measurement accuracy is "Kp", defined as the normalized standard deviation of σ^0, which is a measure of radiometric resolution of the scatterometer, expressed in percentage. The radiometric resolution of the instrument indicates the ability of the sensor to differentiate the backscattered energy. A general goal in scatterometer design is to minimize the Kp value (Naderi et al. 1991). In this way each σ^0 value is described by the accuracy at which it has been measured.

In the ESCAT processing sequence, the standard deviation of σ^0 is calculated as following:

$$Kp = \frac{1}{\sqrt{M}}\left(1+\frac{\sigma^0_{noise}}{\sigma^0}\right) \qquad (2\text{-}1)$$

where M is the number of independent σ^0 measurements and σ^0_{noise} is the σ^0 equivalent of the receiver noise power (Lecomte 1998).

Fig.2-1 shows Kp mean values of mid-beam averaged over the year 1996. Fig.2-2 indicates the frequency distribution of Kp values for each scatterometer antenna triplet.

We should bear in mind that Kp value is a measure of instrument efficiency and does not reflect the noise of geophysical parameter measurements. Therefore a noise model appropriate to the geophysical function is needed to consider the most probable error sources associated with retrieval parameters..

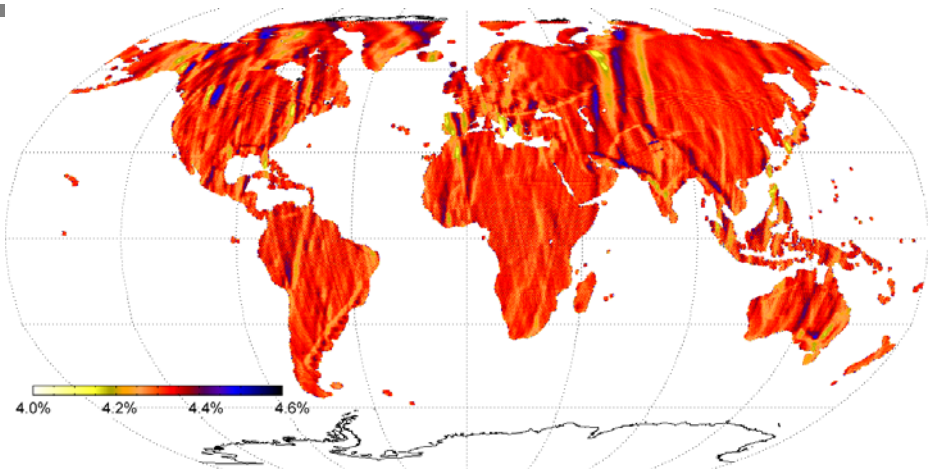

Figure 2-1.

Mean of mid-beam kp measurements of the year 1996

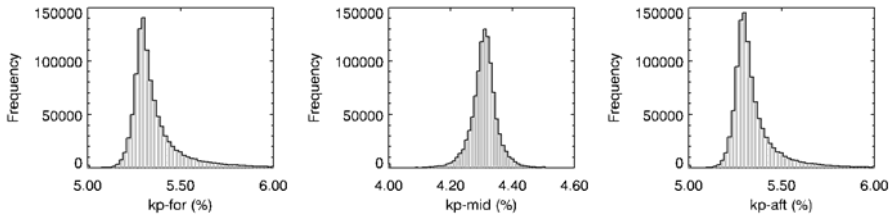

Figure 2-2.

Frequency distribution of Kp values for each scatterometer triplet.

2.2 Noise Model

The backscattering coefficient σ^0, measured by scatterometers, depends on the surface roughness, texture, moisture, and incidence angle of RF signals (Dobson and Ulaby 1986). The relation between soil moisture and σ^0 can be estimated knowing the behavior of σ^0 versus incidence angle and assuming that surface roughness and texture are stable over the time.

The soil moisture retrieval method presented by TU Wien is a change detection approach using a model based on the slope $\sigma'(\theta)$ of the backscattering measurements (Wagner 1998). The slope variable accounts for backscattering variation with incidence angle, which is defined as:

$$\sigma'(\theta) = \frac{d\sigma^0(\theta)}{d\theta} \tag{2-2}$$

The incidence angle behavior of $\sigma^0(\theta)$ is used to extrapolate scatterometer measurements to a reference incidence angle. In this way, the normalized backscattering coefficient will contain information about soil state. But the prerequisite of stable soil roughness is not the only necessary condition. The look direction of the sensor to the surface is also important, which introduces the azimuthal effect problem. Depending on the type of surface roughness, the azimuthal behavior of

a surface varies. The azimuthal dependency of σ^0 encompasses the most probable error sources which have an impact on the soil moisture retrieval procedure of the TU Wien geophysical model. Consequently, an error model based on azimuthal dependency was developed, comprising the most uncertainties of soil moisture estimation. However snow cover and frozen soil can also generate uncertainties in σ^0. Since the behaviour of snow and frozen soil in scatterometer measurements are not well noticeable therefore such conditions must be masked using external datasets.

2.2.1 Azimuthal Anisotropy

As it pointed out above, the backscattering from rough surfaces depends on the azimuthal look direction. Two of three side looking antennas of ESCAT (the same for ASCAT onboard of METOP but on both sides) look at the surface with the same incidence angle but from two different azimuth angles. Discrepancy between fore and aft backscattering coefficients indicates azimuthal dependency plus the noise level of the individual σ^0 measurements (Early and Long 1997).

$$\delta = \sigma^0_{for} - \sigma^0_{aft} \tag{2-3}$$

where σ^0_{for} and σ^0_{aft} denote for fore and aft beam antenna measurements respectively. If a large number of backscattering pairs (fore and aft beam) are available, then the average of δ can be used as an indication of surface anisotropy. Since both fore and aft beams have equal incidence angles, $\delta = 0$ for an isotropic medium.

2.2.2 Estimated Standard Deviation of σ^0

The major sources of noise in soil moisture retrieval with scatterometers can be categorized as following:

- Uncertainties in individual backscattering signals in the receiver (communication noise).
- Uncertainties in the geometry, gain parameters, and resampling of measurements (signal retrieval noise).
- Uncertainties associated with the geophysical model function.

The noise model of WARP5.0 is based on the anisotropic behavior of σ^0 measurements including most parts of the mentioned uncertainties. The error propagation in the model initiates with δ values, which has the advantage of excluding backscattering variations due to the geophysical characteristics of the target since the geophysical induced variations of backscatter appear similarly in both fore and aft beams. In this way δ reflects the noise of independent measurements, which are Gaussian random variables, in addition to the noise caused due to

the surface anisotropy and other possible retrieval errors like speckle and geolocation errors. Geolocation errors may occur because the fore and aft beam antennas do not illuminate exactly the same area because of different antennas patterns on the ground. Uncertainties related to the geophysical model will appear in the noise model after propagating the noise of δ in the soil moisture retrieval algorithm.

An inverse error propagation for measured values of δ is used to estimate the actual noise of the backscattering coefficient σ^0. In other words, we measure uncertainties in the dependent variable δ, which is carried over the uncertainties in the independent variables σ^0_{for} and σ^0_{aft}, to estimate the noise of σ^0.

The following approximation known as the error propagation equation (Bevington and Robinson 2003), is applied for $\delta\left(\sigma^0_{for},\sigma^0_{aft}\right)$. It estimates the error of the dependent variable δ, knowing the error of the independent variables σ^0_{for} and σ^0_{aft}.

$$\mathrm{var}(\delta) \approx \mathrm{var}\left(\sigma^0_{for}\right)\left(\frac{\partial\delta}{\partial\sigma^0_{for}}\right)^2 + \mathrm{var}\left(\sigma^0_{aft}\right)\left(\frac{\partial\delta}{\partial\sigma^0_{aft}}\right)^2 + \ldots. + 2\times\mathrm{covar}\left(\sigma^0_{for},\sigma^0_{aft}\right)\left(\frac{\partial\delta}{\partial\sigma^0_{for}}\right)\left(\frac{\partial\delta}{\partial\sigma^0_{aft}}\right) + \ldots \quad (2\text{-}4)$$

In general, the first two terms dominate the uncertainties. The third term is the average of the cross terms involving products of deviations in σ^0_{for} and σ^0_{aft}, weighted by the product of the partial derivatives. On average, we should expect the third term to vanish in the limit of a large random selection of observation since σ^0_{for} and σ^0_{aft} are independent measurements and uncorrelated, exclusive of soil moisture variations. Considering equation (2-3), equation (2-4) then reduces to (2-5) keeping in mind that all three scatterometer beams have the same noise level:

$$\mathrm{var}\left(\sigma^0\right) = \mathrm{var}\left(\sigma^0_{for}\right) = \mathrm{var}\left(\sigma^0_{aft}\right), \text{ and } \partial\delta/\partial\sigma^0_{for} = -\partial\delta/\partial\sigma^0_{aft} = 1$$

$$\mathrm{var}\left(\sigma^o\right) = \frac{\mathrm{var}(\delta)}{2} \quad (2\text{-}5)$$

Subsequently, the estimated standard deviation of σ^0 is formulated as the standard deviation of δ divided by the square root of 2:

$$ESD(\sigma^0) = \frac{StDev(\delta)}{\sqrt{2}} \quad (2\text{-}6)$$

This is an estimate of the real standard deviation of the backscattering signal. We call it Estimated Standard Deviation because the fore and aft beam antennas illuminate one point on the earth's surface only

from two specific azimuth angles from 360°. But in practice we approach this assumption using multi-year data including both ascending and descending passes. Fig. 2-3-a, b indicate the accuracy extent of this assumption showing the number of measurements available for calculating the ESD and the availability of equal ascending and descending passes at each grid point.

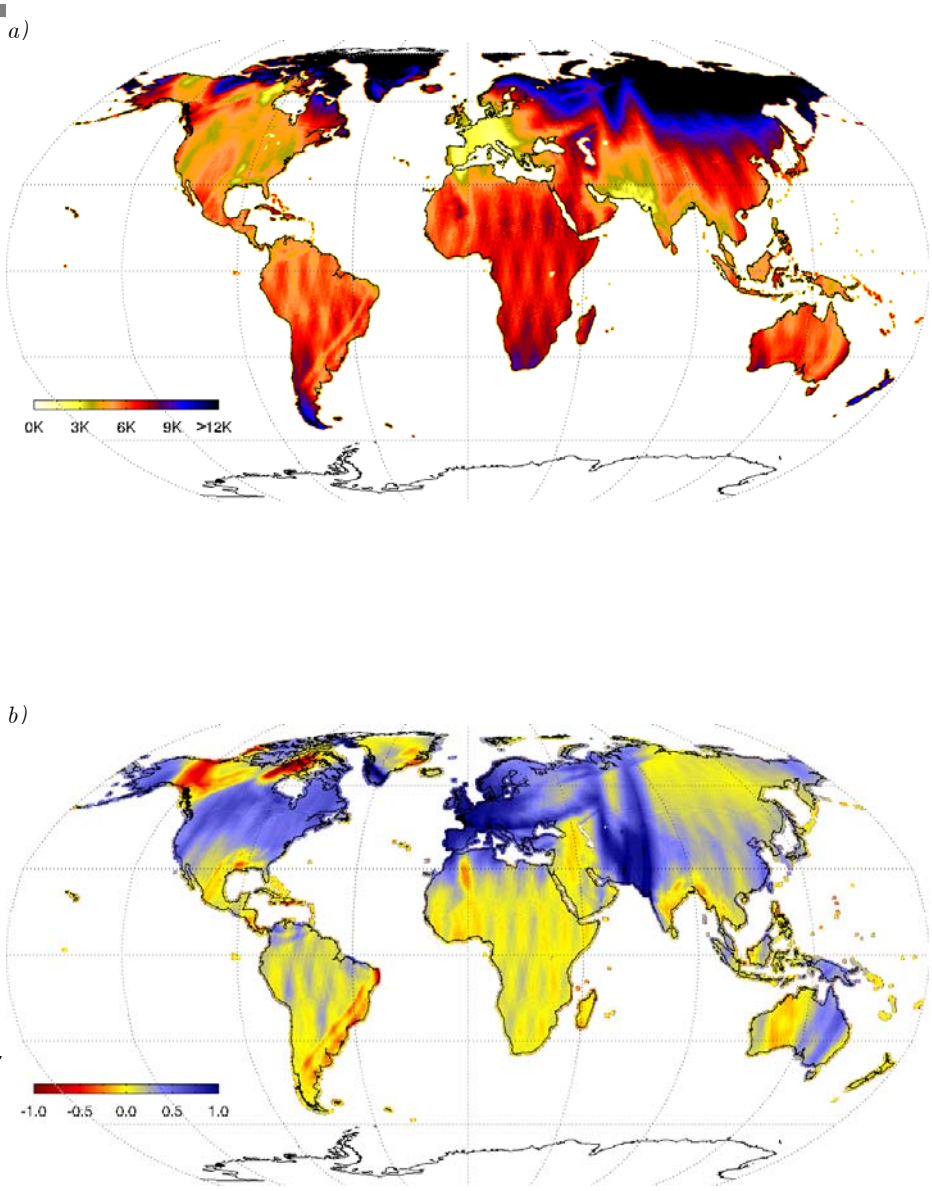

Figure 2-3.

a) Number of measurements available in DGG points.

b) Normalized difference between number of ascending and descending measurements:

$$\frac{N_{ascending} - N_{descending}}{N_{ascending} + N_{descending}}$$

2.2.3 Spatial Correlation of Measurements

Spatially independent data show the same variability regardless of the location of data points. However, spatial data in most cases are not spatially independent. Data values, which are spatially close together show less variability than data values which are farther away from each other. Existing spatial correlation in a dataset characterizes the spatial continuity or roughness of a dataset. In case of existing spatial correlation, the estimated variance could be an underestimation of the

true error of measurements. This should be considered when estimating parameters and related errors in a spatially distributed dataset.

The scatterometer data are resampled to WARP5.0 grid points within an area of 36 km radius around each DGG point. A description of the DGG (discrete global grid) and the resampling procedure used for WARP5.0 were described by (Kidd 2005) and (Bartalis 2005). After the resampling procedure, the measurements are spatially distributed within the resampling area. The presence of spatial autocorrelation in δ values in equation 2-6 may violate the assumption of independency among samples. Fig. 2-4-a and 2-4-b show the δ values of several ascending passes within the resampling area of two different DGG points.

Equation 2-5 known as the semivariogram equation was used to assess the existence of spatial correlation between δ values.

$$\zeta = \frac{1}{2n}\sum[\delta(x) - \delta(x+h)]^2 \qquad (2\text{-}7)$$

where h is the distance between two paired samples, x and $x+h$ denote the positions of two sample pairs and n is the number of pairs.

The semivariogram in Fig. 2-4-c indicates a strong spatial correla-

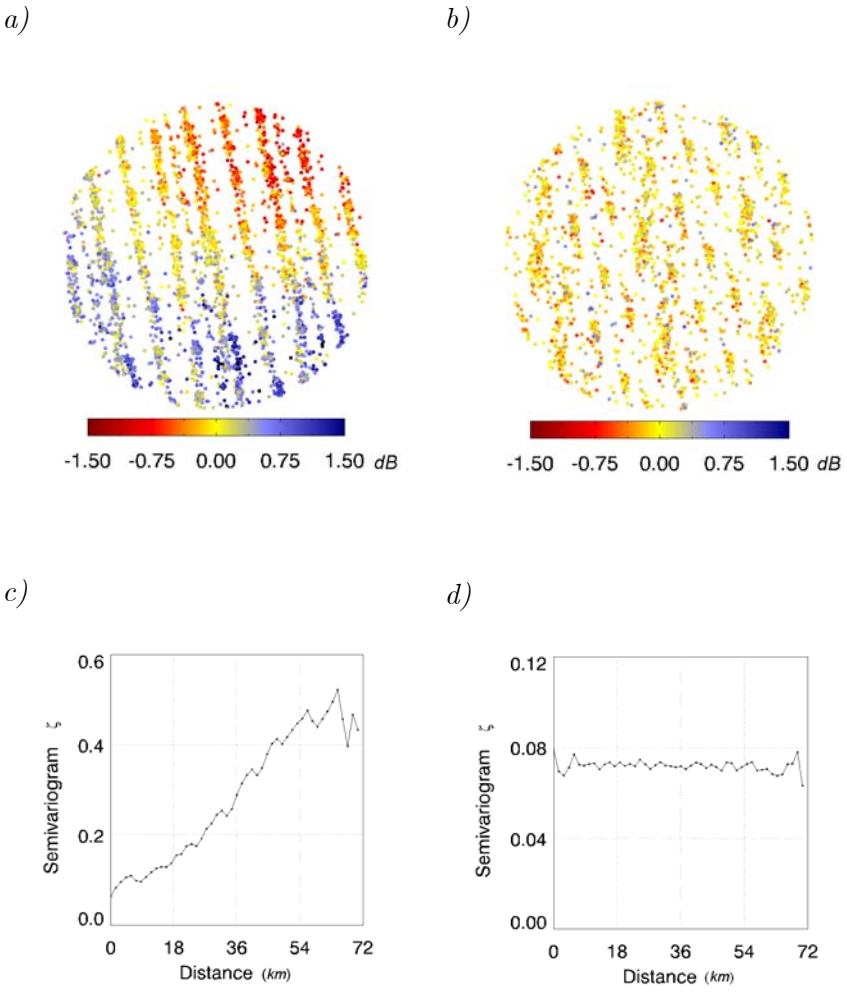

Figure 2-4.

δ measurements within two different grid points where the values are spatially

a) Correlated

Longitude: 84.7139°E

Latitude: 31.6227°N

b) Not-correlated

Longitude: 85.0512°E

Latitude: 26.2092°N

c and d show the semivariograms of a and b respectively.

tion between δ values. The samples which are spatially close together show less variability than those which are far away from each other. Conversely, the samples in Fig. 2-4-d show almost equal variations in all distances.

Spatial correlation might be due to a certain pattern on the surface or definitely an oversampling of the measurements in neighboring nodes during the processing chain of the backscattering signal. To examine the last assumption, an autocorrelation procedure was performed between ESCAT measurements over the rainforests.

Rainforest acts almost like an isotropic surface for scatterometer backscattering. It behaves as a volume scatterer over a wide range of incidence angles. The transmitted signal is equally scattered in all directions. The most of scattered radiation of the incident radar frequencies used in remote sensing satellites and many airborne systems, which operate at X, C and L-band, is from the crown area and tend to have a slow incidence angle θ_{inc} variation which can be characterized by the following equation (Hawkins et al. 1999):

$$\gamma = cons\tan t = \sigma^0 / \cos\theta_{inc} \qquad (2\text{-}8)$$

The signal processing of ESCAT is done for each frame of 19×19 nodes of measurements. Any oversampling of measurements should be detectable using autocorrelation of the measurements in a frame. But no evidence of correlation was found between δ values in scatterometer measurements. Autocorrelation results do not show any significant correlation between δ measurements (Fig. 2-5). However in some cases, γ measurements reveal slight correlation along range direction (Fig. 2-6, 2-7). But this type of correlation is due to natural geophysical correlation between γ values and not because of oversampling. As another example of existing natural correlation even between γ values is the strong correlation found between local precipitation over tropical rainforest in Guyana and the backscattered signal (Woodhouse et al. 1999). The γ values even over the rainforests thus do not always remain constant.

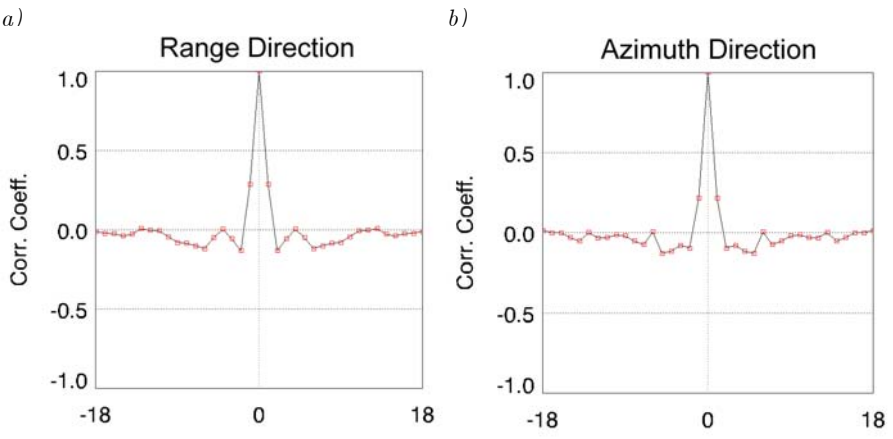

Figure 2-5.
Autocorrelation in:
a) Range direction
b) Azimuth direction
calculated for δ values within a ESCAT frame centered at:
longitude:55.3910°W
latitude:0.1480°N

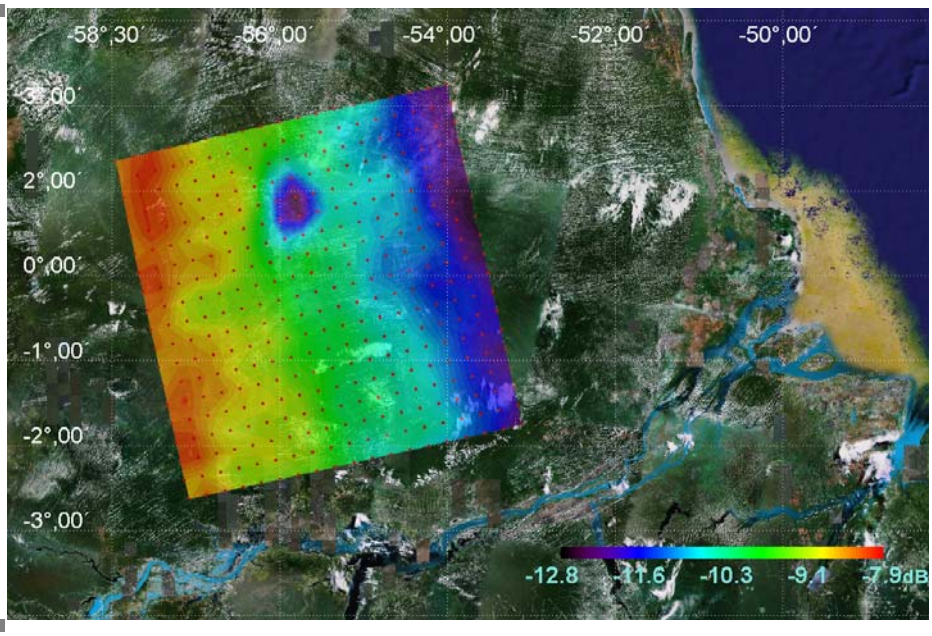

Figure 2-6.

γ values within a ESCAT frame measured on 24.10.1996

Cycle:f2w40961
Orbit:2W07901_.031
Frame:51

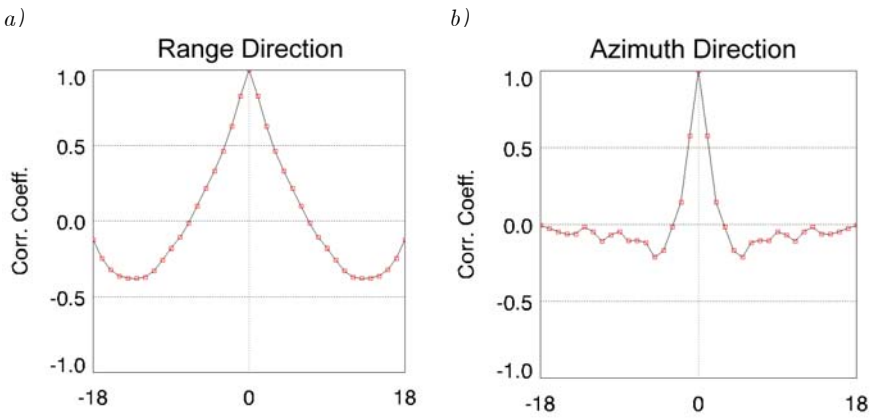

Figure 2-7.

Autocorrelation in:
a) Range direction
b) Azimuth direction
calculated for γ values within a ESCAT frame centered at:
longitude:55.5405°W
latitude:0.8175°N

The microwave dielectric constant of dry vegetative matter is much smaller than the dielectric constant of water. Since a vegetation canopy is usually composed of more than 99% air by volume, the canopy can be modeled as a water cloud whose droplets are held in place by the vegetative matter. Therefore the backscattering coefficient is a function of: volumetric moisture content of the soil, volumetric water content of the vegetation, and plant height (Attema and Ulaby 1978). In case of precipitation over a dense vegetative area, the number of water droplets located on the vegetation canopy increases which this consequently intensifies the backscattering of the canopy. Annual variations in γ measurements were also observed by (Hawkins et al. 1999) in ERS-2 scatterometer data, which were thought to be geophysical in nature. Hence we can evidently conclude that the spatial correlation observed in ESCAT measurements is not related to oversampling of the measurements in neighboring nodes, but occurs due to geophysical effects. Furthermore, the spatial correlation, which was monitored in δ meas-

urements in a number of DGG resampling areas, is also cause by certain natural features like lakes, sand-dunes, or mountains. As a result, the effect of spatial correlation of scatterometer measurements if any is negligible in noise calculations.

2.2.4 Using Hamming Window in ESD Calculations

As mentioned above, the δ values are spatially distributed within the search radius area of each DGG point. In signal processing, a common way of resampling such irregularly distributed data is using a window function (or apodization function) that is zero valued outside of a chosen interval. When the data signal is multiplied by the window function, the product is also zero-valued outside the interval. All that is left is the "view" through the window. Hamming window is a window function frequently used in radar remote sensing, described as:

$$H(x) = 0.54 + 0.46\cos\left(\frac{\pi x}{r}\right) \tag{2-9}$$

where x is the distance to the centre of the window and r is the radius of the window (Blackman and Tukey 1959). The Hamming window is a weighting function, which assigns more weight to the points closer to its centre value and less to those further away.

In the signal noise processing of WARP5.0, δ values measured during each satellite pass (equal orbit), are averaged within the resampling area with a radious of 36km using the following the Hamming window function:

$$\delta_H = \frac{\sum_{i=1}^{m} \delta_i \cdot H(x_i)}{\sum_{i=1}^{m} H(x_i)} \tag{2-10}$$

where m is the number of δ measurements during each satellite pass and δ_H denotes the weighted value of δ using the Hamming function.

Through the Hamming window, δ_H represents a more stabilized character of the resampling area. Spatial features, like those presented in Fig. 2-4-a, are also eliminated after the Hamming function implementation. Considering equation (2-6), the estimated standard deviation of σ_H^0 (weighted value of σ^0) is as following:

$$ESD(\sigma_H^0) = \frac{StDev(\delta_H)}{\sqrt{2}} \tag{2-11}$$

$ESD(\sigma_H^0)$ is the noise parameter which is used in error propagation of WARP5.0 (Fig 2-8). In the soil moisture retrieval algorithm, the same window function is also used for each three scatterometer beams

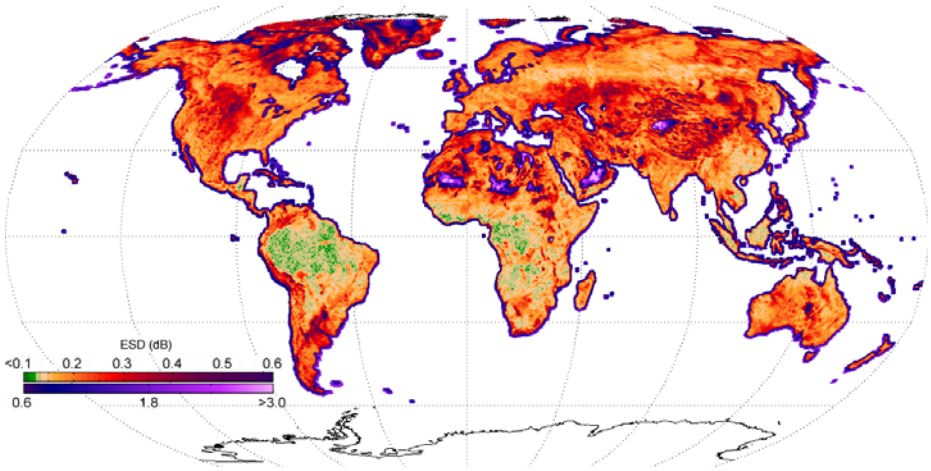

Figure 2-8.
Estimated Standard Deviation of σ_H^0

within the resampling area for each satellite pass to obtain a unique soil moisture value assigned to each DGG point.

2.2.5 Noise of Azimuthally Corrected Measurements

In the WARP5.0 processing algorithm, the noise of measurements, which reveal high azimuthal effects, is reduced partly using an azimuthal correction method (Bartalis 2005) and (Hasenauer et al. 2006). Triplets of the backscattering measurements are split up to six groups of σ_{for}^0 , σ_{mid}^0 , and σ_{aft}^0 for each ascending and descending passes plus a seventh group including the whole measurement time series. The backscattering measurements in each group are considered as a function of their incidence angles. After eliminating outliers, a second-order polynomial function is applied to measurements in each group. For each individual measurement, the difference between the function value of the relative group and the function value acquired from the whole back scattering measurements at the same incidence angle, is considered as a correction factor. Fig. 2-9 shows $ESD(\sigma_H^0)$ values after azimuthal cor-

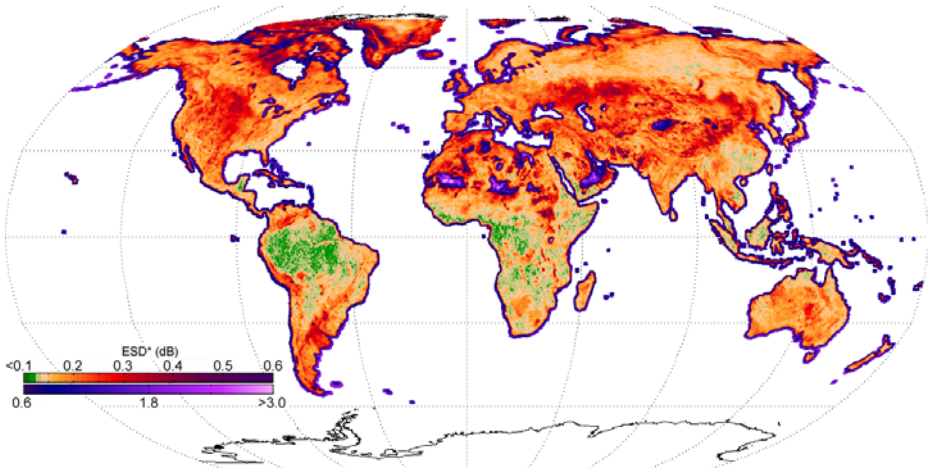

Figure 2-9.
Estimated Standard Deviation of σ_H^0 *after azimuathal correction*

rection. Frequency distributions of different versions of $ESD(\sigma^0)$ are shown in fig. 2-10.

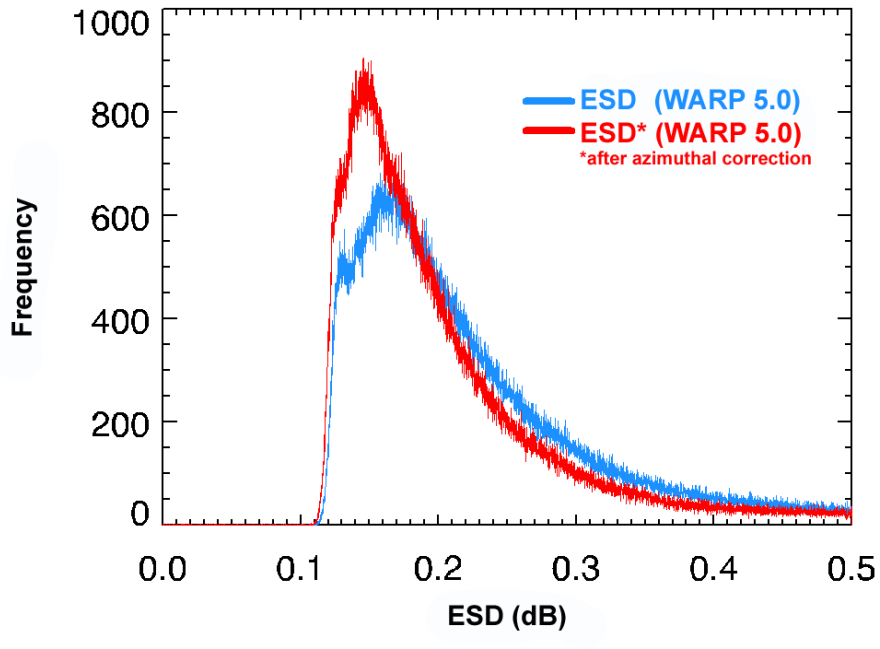

Figure 2-10.
Comparing Frequency Distributions of $ESD(\sigma_H^0)$ *and* $ESD(\sigma_H^0)^*$

3 Error Sources Definition

In the following sections the factors, which have the most important impact on the δ measurements, are discussed. Identification of the error sources and the magnitude of their effects on the scatterometer measurements will improve our understanding about the parameters generated by the geophysical model function during the WARP5.0 retrieval process.

3.1 Instrument Noise

In addition to ground-based transponders which are generally used to calibrate scatteromer measurements, one solution for measuring instrument noise is measuring backscattering coefficients over the rain forests. Rainforests in microwave radiations at X, C, and L-band, behave as a volume scatterer over a wide range of incidence angles. The transmitted signal is equally scattered in all directions. Hence the Amazon rainforest has been chosen as the reference natural target in some Earth Observation missions like ERS-1, ERS-2, J-ERS-1, and RADARSAT (Crapolicchio and Lecomte 2003).

The difference between σ^0_{for} and σ^0_{aft} measurements over rainforest areas can be approximated as the noise of the instrument. The instru-

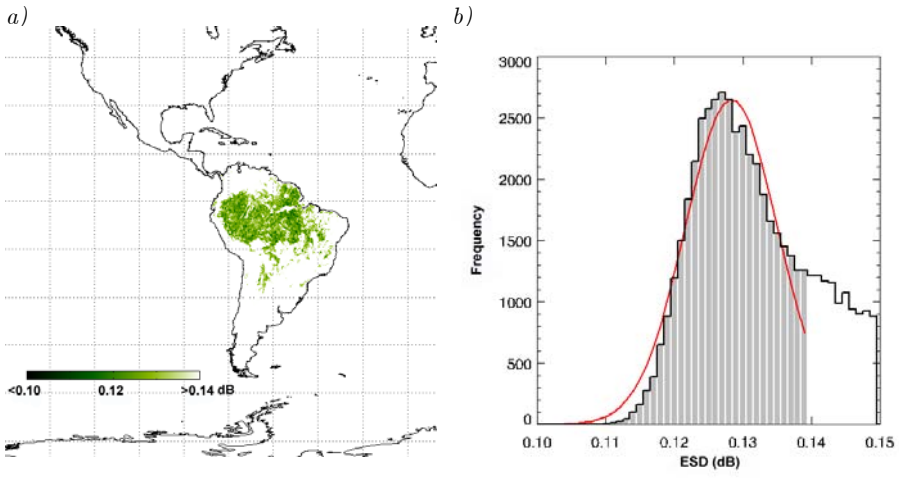

Figure 3-1.

a) Spatial distribution of DGG points with ESD values less than 0.14.

b) Frequency distribution of ESD values of theselected DGG points in fig. a.

ment noise is a random variable with a normal distribution and is independent of geophysical characteristics of the surface. To estimate the instrument noise, an area over the Amazon rainforest is chosen (DGG points) which have *ESD* values below 0.14dB. This area covers most parts of the Amazon rainforest with the densest vegetation (Fig.3-1-a). Considering the frequency distribution of these 41871 DGG points with *ESD* values below 0.14dB (Fig.3-1-b), the average of the *ESD* can be an approximation of instrument noise which is about $0.13 \pm 0.01 dB$.

3.2 Geophysical Error Sources

The backscattering coefficient is dependent on the portion of the transmitted energy that is returned back to the radar from targets on the surface. The magnitude or intensity of this backscattered energy depends on how the radar signal interacts with the surface. Thus the geometry of scatterometer beam is as important as the geophysical parameters of the surface. The relationship between viewing geometry and the geometry of the surface features plays an important role in how the radar energy interacts with targets and their corresponding backscattered energy.

3.2.1 Mountains

When the scatterometer beam reaches the base of a slant features like mountains tilted towards the satellite, the local incidence angle of fore and aft beam will be different depending on the look angle of the scatterometer and the slope of the mountain. Maximum differences occur when the satellite track is perpendicular to the slope. Mountain ridges with different slope sharpness on each side cause clearly opposite δ values during ascending and descending passes (see Fig. 3-2).

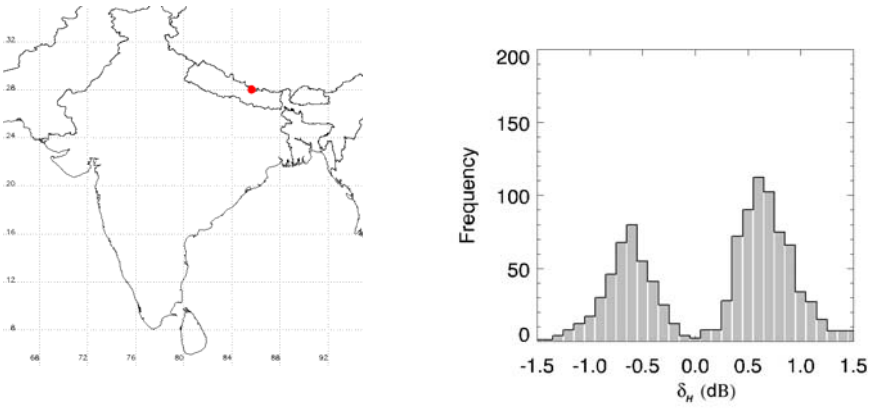

Figure 3–2.

Distribution of δ_H (fore-aft) values for a selected DGG point located in Himalaya mountain range.

The positive values are observed in ascending and the negative values in descending passes.

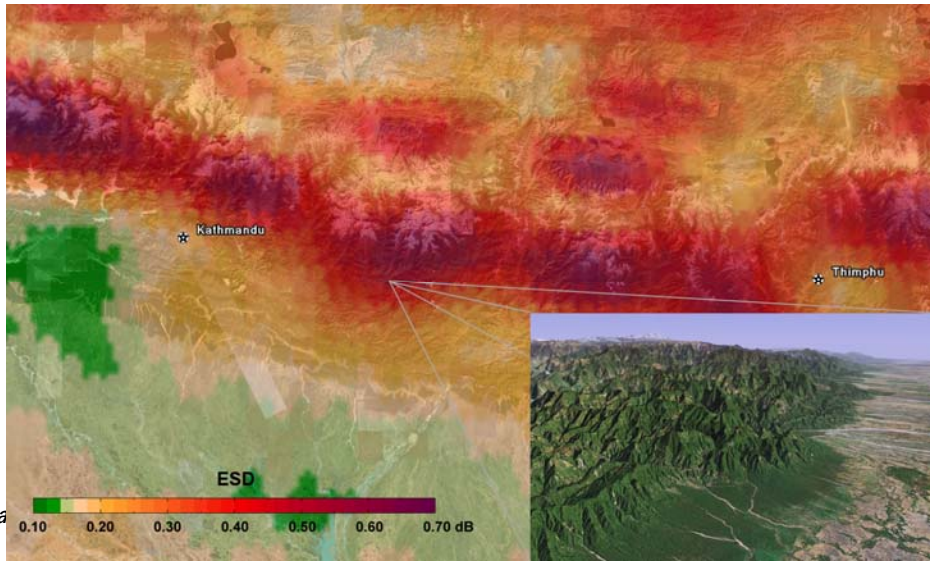

Figure 3–3.

Shows ESD values over Himalaya mountain ranges.

If the look direction is close to perpendicular to the orientation of the feature, then a large portion of incident energy will be reflected back to the sensor. The more oblique look direction in relation to the feature orientation, the less energy will be returned to the sensor. The look direction can significantly influence the appearance of features, particularly when ground features are organized in a linear structure, such as mountain ranges. Fig. 3-3 shows *ESD* values over steep mountainous terrain.

3.2.2 Water

Backscattering from water depends on the roughness of the water surface. When the water surface is calm then specular reflection occurs and σ^0 is very low. Opposite, wind generates water waves spread out

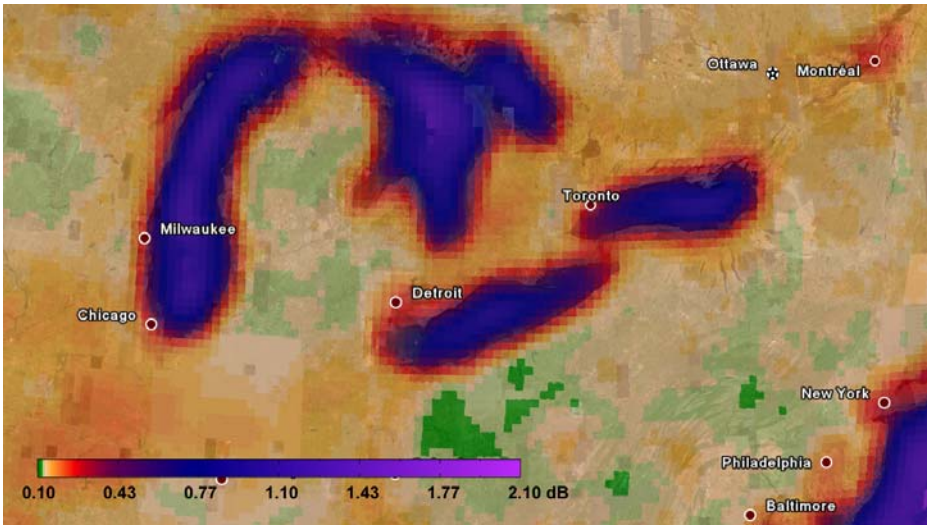

Figure 3–4.

Shows ESD values of Great Lakes in northern America.

across the surface that increase scattering in backward direction. The difference between fore and aft beam backscatter is maximum when the radar looks into the upwind or downwind direction. The main contributions do not come from large waves, even if they are many meters height. Rather, scattering is dominated by little water ripples on the surface (Ulaby et al. 1982). Fig. 3-4 shows *ESD* values over the Great Lakes in northern America.

In addition to the large water reservoirs, shallow bodies of water like swamps, marshes, estuaries, rivers and any set of small bodies of water cause different backscattering in fore and aft direction. The range of *ESD* depends on the extend of the water body in comparison with spatial resolution of scatterometer and the roughness of water surface, which is related to the water flow and wind strength. Fig 3-5 shows *ESD* values over an area in Bangladesh encompassing many small ponds and rice farms. The area is also categorized as flood plain (Fig. 3-6). Large and spread out rivers like the Amazon river have also a significant influence on *ESD* values, although the land cover of riverside plays an important role in total backscattering (Fig. 3-7).

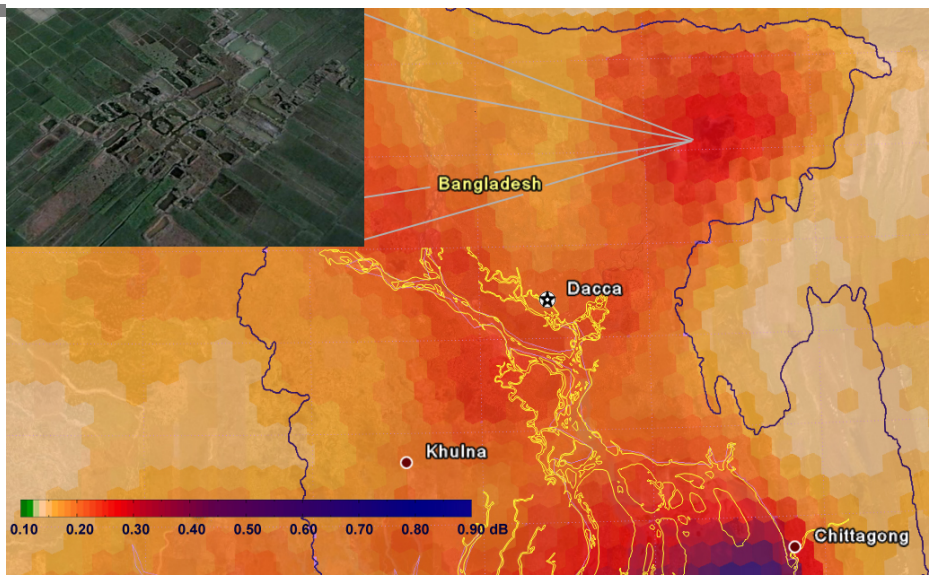

Figure 3–5.

Shows ESD values over an area in Bangladesh comprising rice farms and several small water bodies.

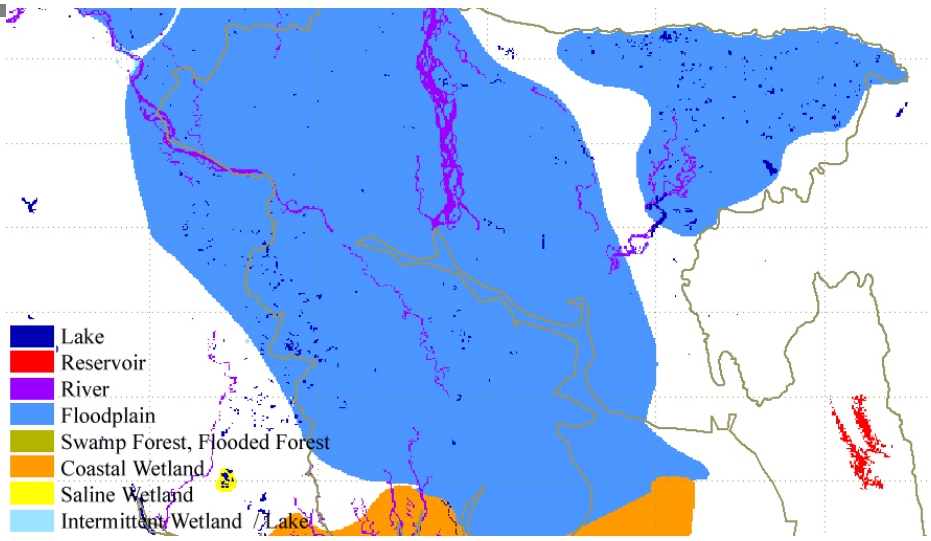

Figure 3–6.

Lakes and wetlands map of the area shown in fig. 3-5 (Lehner and Doell 2004).

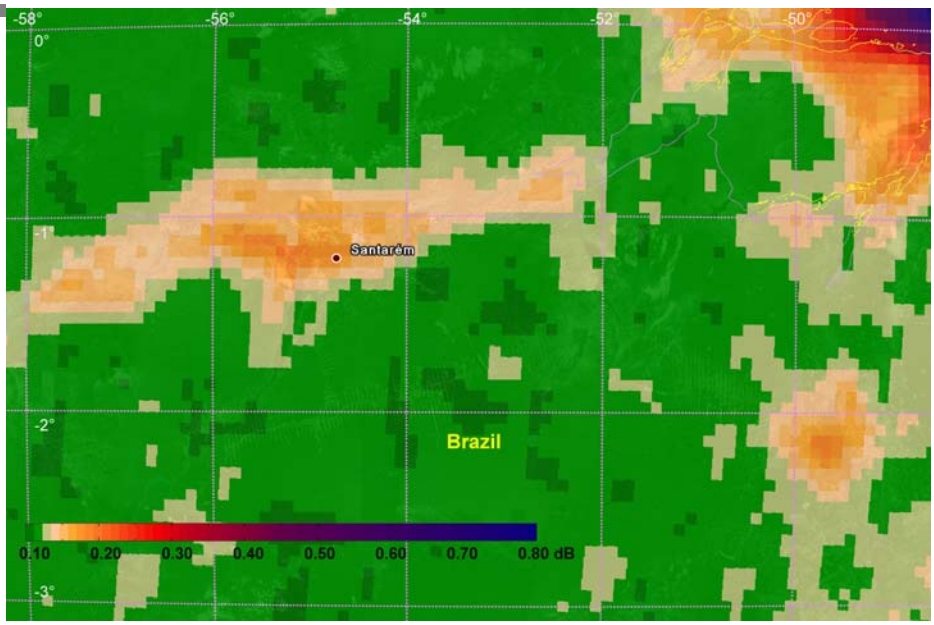

Figure 3–7.

Shows ESD values over the Amazon river basin.

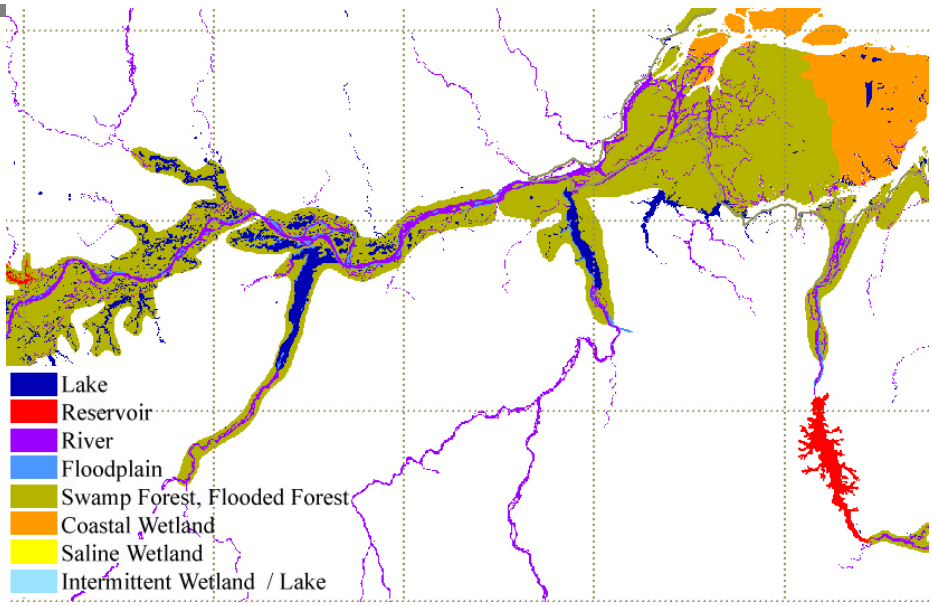

Figure 3–8.

Lakes and wetlands map of the area shown in fig. 3-7 (Lehner and Doell 2004).

3.2.3 Desert Dunes

The same anisotropy like the one found over the open water is also observable over sand desert areas. Wind erosion in large sand areas is similar in many ways to how wind interacts with the ocean surface, how water transports sediments on a river bed or how snow drifts (Bagnold 1941). However, asymmetric backscatter response of the sand areas is more complicated. The interaction of microwaves with such sand features may happen not only in the surface layer of the matter but also in the deeper layers in form of volume scattering. Moreover the azimuthal response is sensitive to the orientation of small-scale (millimetres to meters) wind induced sand ripples, rather than the lar-

ger scale dune orientation (Bateson and Woodhouse 2004). Fig. 3-9 shows *ESD* values over the Taklamakan sand desert in Central Asia.

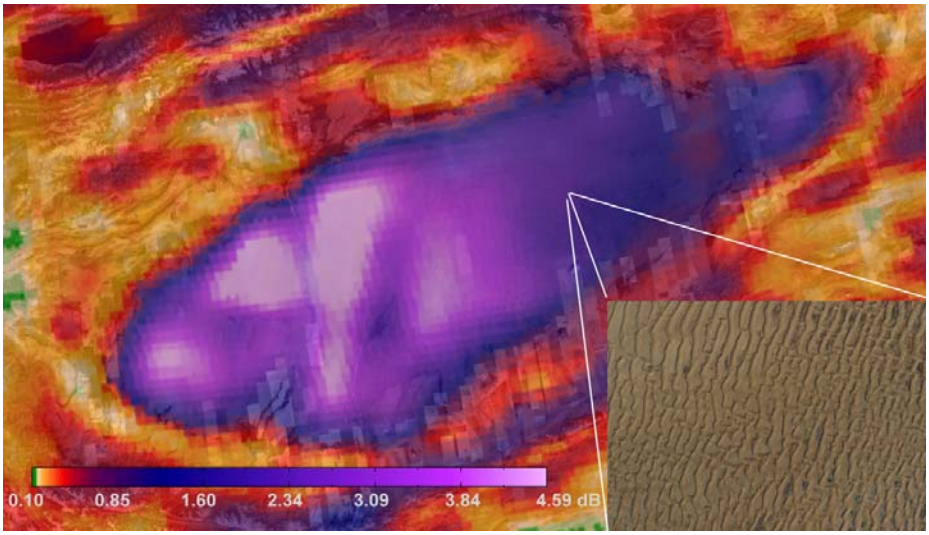

Figure 3–9.

Shows ESD values over the Taklamakan desert in Central Asia which is known as the largest sand-only desert in the world.

Bibliography

Attema EPW (1991) The Active Microwave Instrument on-board the ERS-1 satellite. Proceedings of the IEEE 79:791

Attema EPW, Ulaby FT (1978) Vegetation Modeled as a Water Cloud. Radio Science 13:357

Bagnold RA (1941) The Physics of Blown Sand and Desert Dunes. In. Methuen & Co., London

Bartalis Z (2005) Selection of Resampling Procedure. ASCAT Soil Moisture Report Series, No. 6. In. Institute of Photogrammetry and Remote Sensing, Vienna University of Technology, Vienna, Austria

Bateson, Woodhouse (2004) Observations of scatterometer asymmetry over sand seas and derivation of wind ripple orientation. International Journal of Remote Sensing 25:1805

Bevington PR, Robinson DK (2003) Data reduction and error analysis for the physical sciences, 3 edn. MacGraw-Hill, New York

Blackman RB, Tukey JW (1959) Particular pairs of windows. In: The measurement of power spectra from the point of view of communications engineering, New York: Dover, pp pp. 98-99

Crapolicchio R, Lecomte P (2003) On the stability of Amazon rainforest backscattering during the ERS-2 Scatterometer mission lifetime. In: ASAR workshop 2003, Canada

Dobson MC, Ulaby FT (1986) Active Microwave Soil Moisture Research. IEEE Transactions on Geoscience and Remote Sensing GE-24:23

Early DS, Long DG (1997) Azimuthal modulation of C-band scatterometer over Southern Ocean sea ice. IEEE Transactions on Geoscience and Remote Sensing 35:1201

Hasenauer S, Scipal K, Naeimi V, Bartalis Z, Wagner W (2006) WARP 5.0 Software Documentation, ASCAT Soil Moisture Report Series, No. 13. In. Institute of Photogrammetry and Remote Sensing, Vienna University of Technology, Austria, Vienna

Hawkins R et al. (1999) Stability of Amazon Backscatter at C-band: Spaceborne Results from ERS-1/2 and RADARSAT-1. In: CEOS SAR Workshop. ESA-SP450

Kidd R (2005) Discrete Global Grid Systems. ASCAT Soil Moisture Report Series, No. 4. In. Institute of Photogrammetry and Remote Sensing, Vienna University of Technology, Vienna

Lecomte P (1998) The ERS scatterometer instrument and the on-ground processing of its data. Proceeding of Emerging Scatterometer Application Workshop ESTEC, Noordwijk, the Netherlands 5-7 October 1998:241

Lehner B, Doell P (2004) Development and validation of a global database of lakes, reservoirs and wetlands. Journal of Hydrology 296:1-22

Naderi FM, Freilich MH, Long DG (1991) Spaceborne radar measurement of wind velocity over the ocean--An overview of the NSCAT scatterometer system. Proceedings of the IEEE 79:850

Naeimi V (2007) WARP5.0 Error Analysis 2. ASCAT Soil Moisture Report Series, No. 12. In. Institute of Photogrammetry and Remote Sensing, Vienna University of Technology, Vienna, Austria

Ulaby FT, Moore RK, Fung AK (1982) Radar Remote Sensing and Surface Scattering and Emission Theory. Artech House, Norwood, MA

Wagner W (1998) Soil Moisture Retrieval from ERS Scatterometer Data, dissertation. In: Institute for Photogrammetry and Remote Sensing. Vienna University of Technology, Vienna, p 111

Woodhouse IH, van der Sanden JJ, Hoekman DH (1999) Scatterometer observations of seasonal backscatter variation over tropical rain forest. IEEE Transactions on Geoscience and Remote Sensing 37:859